ISSN 1330-3651 (Print), ISSN 1848-6339 (Online)
https://doi.org/10.17559/TV-20220111154304
Original scientific paper

Tribological Properties of Medical Material (MED610) Used in 3D Printing PJM Technology

Mateusz RUDNIK, Muammel M. HANON, Wiktor SZOT, Karolina BECK, Damian GOGOLEWSKI, Paweł ZMARZŁY, Tomasz KOZIOR*

Abstract: The development of modern manufacturing technologies related to the ongoing industrial revolution Industry 4.0, is largely related to the dynamic development of materials chemistry. This means that currently 3D printing technologies allow the production of physical models using newer materials with better properties and application in new industrial sectors. The article presents the results of tribological tests of the bio-medical material under the trade name MED610, which shows biocompatibility for medical and dental purposes. The paper presents the results of measurements of tribological models of samples designed and manufactured in the shape of rings. Using the variable friction parameters, the wear process was described in the pressure-rotational speed (*P-V*) system. Moreover, the friction coefficient and wear measured by using the linear method were analyzed. The paper also presents a metrological analysis carried out with the application of an optical profilometer on the surface of the samples after pressing at the contact point of the surface during the test. The preliminary review of the test results showed that the MED610 material exhibited relatively good abrasion resistance. However, it cannot be employed for heavily loaded friction nodes, and in the *PV* diagram even at a relatively small value, the sample models were destroyed.

Keywords: 3D printing; additive manufacturing; MED610; PJM; tribology

1 INTRODUCTION

Additive manufacturing (AM), also known as 3D printing, is a novel manufacturing technology that has abundant potential implementations in research and industry. AM methods create three-dimensional (3D) components directly from CAD models by layering materials (layer by layer), allowing for the creation of parts with free form geometry [14, 17], and decreased product lead times and tooling costs in comparison to traditional machining processes like turning [31, 38]. The characteristics of 3D printed parts can be influenced by structural and process factors rather than just material attributes. Highly anisotropic materials are produced as a result of complex interaction processes, with anisotropy varying both locally inside portions and globally between seemingly identical sections [26]. It should be noted that 3D printing parameters selection is very important because they affect the shape and dimensional accuracy of the manufactured elements [1, 7, 21]. The introduction of new composite materials for 3D printing and new technologies seems to be particularly important in this field [4, 5, 24, 30, 32]. Using 3D printing technologies such as SLS or FDM and PJM, we have the option of building and utilizing many materials enriched with additives [9] that improve functional properties and which so far have not been comprehensively analyzed in the context of tribological tests.

PolyJet modelling (PJM) 3D printing is a promising technology that allows simultaneous jetting of modelling materials to be implemented to create extremely complex physical prototypes with smooth surface and high precision [6, 37]. Its 3D printers have the highest resolution of any commercially accessible 3D printing technology allied with the fewest design limitations. The desired components can be manufactured in this method by a process comprising the addition of photopolymer resin layers [36]. In photopolymerization-based additive manufacturing, when layers of liquid photopolymer resin are exposed to ultraviolet (UV) light, they undergo a chemical process that causes them to solidify. This includes a number of unique characteristics that can affect the physical, chemical and biological aspects of AM-made devices [2]. Considerable efforts were made in previous studies to review the characteristics of the PJM technology products, including, but not limited to the dimensional accuracy [20], rheological features [22], mechanical properties [25, 29, 35], viscoelastic qualities [23], surface roughness [3] and thermal stability [16].

MED610 is a biocompatible, transparent PolyJet material that has been medically approved for physical contact. The material is authorized for persistent skin contact (exceeds 30 days) and restricted mucosal membrane contact (reaching 24 hours) in both dentistry and medical applications [34]. In the literature, several researchers have examined the MED610 material to evaluate its possibility to be employed for various medical applications.

Xin Gong et al. [15] have employed the biocompatible material MED610 for 3D printing of naso-alveolar moulding (NAM) devices, to explore the possibility of a completely digital workflow for presurgical NAM treatment in infants' bilateral and unilateral cleft lip and palate (CLP). For this purpose, design and manufacturing of a consecutive series of customized NAM appliances in advance for the presurgical treatment has been done. The clinical results revealed that this fully digital process was effective, feasible and capable of estimating the treatment goal. By the conclusion of presurgical NAM therapy, the malposition alveolar segments were aligned properly and the surrounding soft tissues were repositioned. This technique has the advantages of being safe, affective and time saving.

In another published study, mussel-inspired aided apatite mineralized on a PolyJet material for synthetic bone scaffold was investigated [8]. Here, the physical characteristics, cell morphology, cell proliferation and alkaline phosphatase (ALP) expression level of the polydopamine /hydroxyapatite coating were evaluated on the printed MED610 objects. The findings demonstrate that the polydopamine/hydroxyapatite coating improves the biocompatibility, hardness and osteogenic differentiation capacity of printed items. Also, the study found that adding a polydopamine/hydroxyapatite coating

to the MED610 biomedical 3D printing material, which has been utilized in the medical field, improved the material's hardness, hydroxyapatite mineralization, good cell morphology, cell proliferation and ALP expression levels. As a result, according to the authors, the polydopamine/hydroxyapatite coating improves the development and potential of MED610 materials for clinical purposes in dentistry and orthopaedics.

Catherine Ngan et al. [27] have optimized the biocompatibility of 3D-printed photopolymer structures in vitro and in vivo. Therein, the cytotoxicity of MED610 photopolymer was considerably reduced due to the development of a sonication technique for repeatable cleaning. This cleaning method does not impair the structural integrity of MED610 structures, making them acceptable for subdermal implantation (for short-term) in the nude rat model. The findings, thus, revealed a more cytocompatibility cleaning process for printable photopolymers, allowing for more creative 3D-printed bespoke designs for cell culture applications in vitro and in vivo.

Although numerous characteristics of PJM printing products were extensively investigated for medical applications, their tribological properties (for most print-compatible materials in general and MED610 in particular) have yet to be determined. In this context, optimization of tribological features is critical, as biocompatible materials within the cultured cell may be damaged owing to the friction and wear during utilization. This was not commonly addressed for PJM materials so far.

In this paper, the tribological properties of PJM made MED610 samples were studied comprehensively. The testing results were mainly utilized for the evaluation of the friction, wear, temperature and pressure-velocity (P.V) properties of MED610 material examined in three different applied loads (30, 45, and 60 N) and velocities (100, 150, and 200 m/s). Furthermore, metrological analysis was also carried out to estimate the reliability of the printing technology and material. To the best of our knowledge, no results are available yet in the literature about the effect of testing parameters on MED610 material's wear and friction. Therefore, this study aims to fill the gap in knowledge surrounding the impact of PJM 3D printing on MED610 tribological behavior. This would help to facilitate picking proper biocompatible materials when using PJM fabricated parts for certain medical applications.

2 MATERIALS AND METHODS

2.1 Samples

The samples were designed using SolidWorks (Dassault Systèmes SolidWorks Corp., Waltham, MA, USA) CAD software according to the manual of a T-15 tribometer. The samples were fabricated using photo-curable liquid polymer resin PolyJet Matrix (PJM) and material based on resin - MED610. Samples were made in number of 27. Technological parameters of 3D printing were: printing direction 0° (flat surface on the building tray) and layer thickness 0.016 mm (high quality mode). The dimensions of the samples are shown in Fig. 1 and the position on the printing platform is shown in Fig. 2.

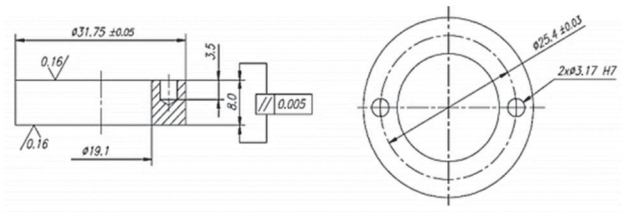

Figure 1 Sample dimensions

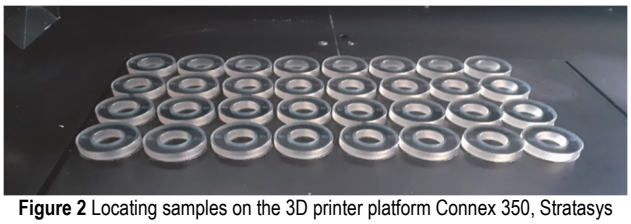

Figure 2 Locating samples on the 3D printer platform Connex 350, Stratasys

2.2 Tribological Research

Tribological tests were carried out on a tribometer T-15 (Łukasiewicz Research Network - The Institute for Sustainable Technologies, Radom, Poland). The research device consists of a T-15 tester, measuring and control systems and a computer with software for analyzing and recording the results (Fig. 3). The kinematic schematic of the T-15 tester works is shown in Fig. 4. The type of device is ring on disc, and contact between the counter sample made of C45 steel and the PJM sample was plane-plane.

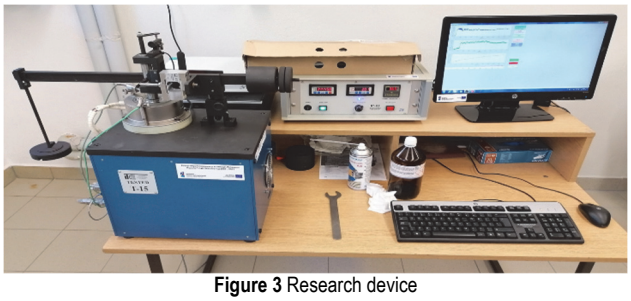

Figure 3 Research device

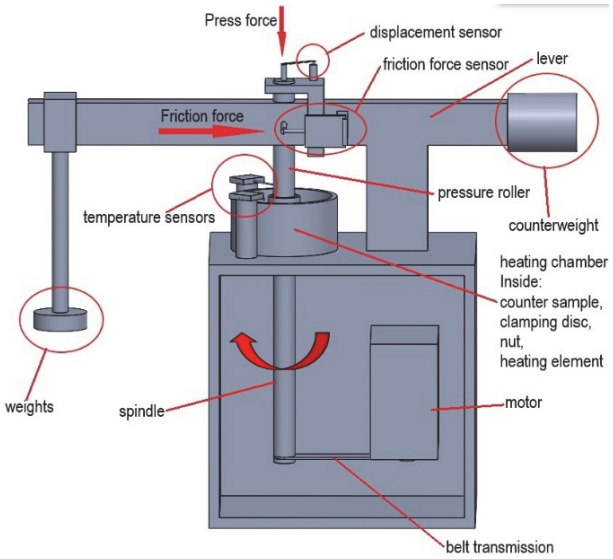

Figure 4 Simplified Tribological Model

The T-15 tester allows for measurement of: linear wear, friction force and temperature in the test chamber and in the loseness of the contact between the counter sample and the sample. Additionally, it is possible to work in a gas

and lubricant environment in a closed chamber. Moreover, the chamber can be heated up to the temperature of 200 °C.

The test duration for all samples was 3600 seconds. The other tribological parameters and determination of the samples are presented in Tab. 1. The measurements were made according to DOE (design of experiment) $X^Y = 3^2$, (9 research type), where X is the number of levels of variation and Y - the number of variable parameters. Each type of test was performed on three identical samples (a, b and c see Tab. 1), which generated a total of 27 tests. The variable parameters were: rotational speed (0.17, 0.25 and 0.34 m/s respectively 100, 150, and 200 (rpm)) and pressure (30, 45 and 60 N).

Table 1 Determination and sample parameters

Sampledetermination	Parameters	
	V/ m/s	*Fn* / N
1a, 1b, 1c	0.17	30
2a, 2b, 2c	0.25	
3a, 3b, 3c	0.34	
4a, 4b, 4c	0.17	45
5a, 5b, 5c	0.25	
5a, 6b ,6c	0.34	
7a, 7b, 7c	0.17	60
8a, 8b, 8c	0.25	
9a, 9b, 9c	0.34	

2.3 Material MED610

The MED610 material is biocompatible and is used with PJM printing technology. The material can be used medically and denstistically. Material MED610 allows continuous contact with the skin for up to 30 days and with the mouth for up to 24 hours. The material was developed according to accepted standards, taking into account: cytotoxicity (EN ISO 10993-5:2009) [13], sensitization and hyper sensitivity type IV (EN ISO 10993-10:2013) [10], genotoxicity(EN ISO 10993-3:2014) [12], chemical characterization (EN ISO 10993-18:2009) [11]. Selected properties are listed in Tab. 2 [34].

Table 2 Properties of MED610 material [34]

Property	Standard	Value
Tensile strength	D-638-03	50 - 65 MPa
Ultimate elongation	D-638-05	10 - 25%
Young's modulus	D-638-04	2000 - 3000 MPa
Bending strength	D-790-03	75 -110 MPa
Modulus of elasticity in bending	D-790-04	2200 - 3200 MPa
Poisson ratio*	ASTM D638-10	0.41
Deflection temperature (under load of 0.46 MPa)	D-648-06	45 - 50 °C
Water absorption	D-570-98 24HR	1.1 - 1.5%
Shore hardness	D Scale	83 - 85 D
Rockwell hardness	M Scale	73 - 76 M
Biocompatibile	PN-EN ISO 10993-1:2017	Skin contact - more than 30 days Mouth contact - up to 24 hours

* Note: the Poisson ratio value was obtained by Stratasys at the authors' request.

2.4 Metrological Research

Metrological tests after tribological research were performed on the Talysurf CCILite device for 20 samples that were not damaged during the tribological test. The Talysurf CCI measuring system is shown in Fig. 5. The measuring instrument is used to perform optical, non-contact measurements and analyses of the geometric structure of a surface. It is equipped with a set of lenses: ×2,5; ×10; ×20; ×50. The system enables the assessment of geometrical structure of the surface with a vertical resolution of up to 0.01 nm. In the measurement, the ×10 objective was used.

Figure 5 Talysurf CCI Lite

The results were processed in the software Mountain Lab, where parameters were determined and operations were undertaken such as:

- maximum depth,
- hole area,
- profile lenght,
- 3D models,
- sample profiles.

Metrological measurements were made at the same wear point at a nominal distance of 5 mm from outside diameter to inside diameter of sample as shown in Fig. 1.

3 RESULTS AND DISCUSSION

3.1 Data Obtained Analysis

During the tests, the measurement device (Spider) was recording the data of three parameters, parallel with the testing time, including friction force, displacement (wear depth) and temperature. The data of these parameters were measured firstly by the designated sensors and then transferred to the computer through the Spider device. The pure data of each sample could be plotted individually versus time, as shown in Fig. 6a to Fig. 6c.

To obtain the coefficient of friction (μ), the frictional coefficient (F) values were divided by the normal applied loads, according to the μ equation ($\mu = F/N$) [18]. As can be seen in the exemplars of the initial graphs of wear depth and friction coefficient (Fig. 6b and Fig. 6d, respectively), the data was quite dense (3600 measurements/points). Such a curve (whether friction or wear) is not suitable for analysis and has no possibility to be placed into a comparison with the curves of other results within one graph. Therefore, the data was filtered, at only 45 (out of 3600) to draw the proper curve. This was achieved by picking one out of each 80 measurements, in other words, the first points of each 80 measurements set were picked,

while the remaining 79 were omitted. This way eliminates the unnecessary oscillations around each point and exhibits the tendency of the curve clearly. The curves presented in Fig. 7 and Fig. 8 show the plotted data after filtration. For reliable results, each testing condition (load and speed) was repeated on three identical samples, and then the average value was determined.

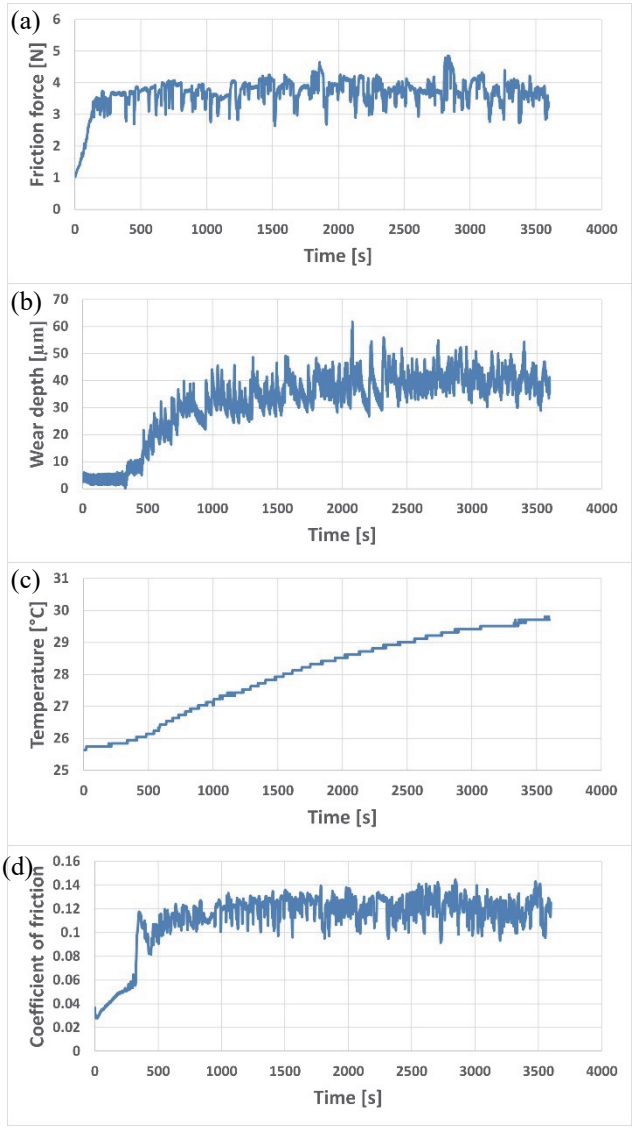

Figure 6 Exemplars of the measured and analysed data after testing (a) friction force, (b) wear depth, (c) temperature and (d) coefficient of friction vs. time

3.2 Tribological Characterization of PJM 3D Printed Parts

As mentioned in the methodology part, the tribological tests were performed under various testing conditions (speed and load). Friction curves always start with the running-in stage, where the friction rises sharply. This occurs because the slip between the surface of the 3D-printed part and the corresponding surface (counterpart) is so far unstable, as the roughness of the sample's surface has not yet been polished [19]. After a while, the curve reaches a steady (uniform) stage where the friction oscillates only around a level approximately convergent.

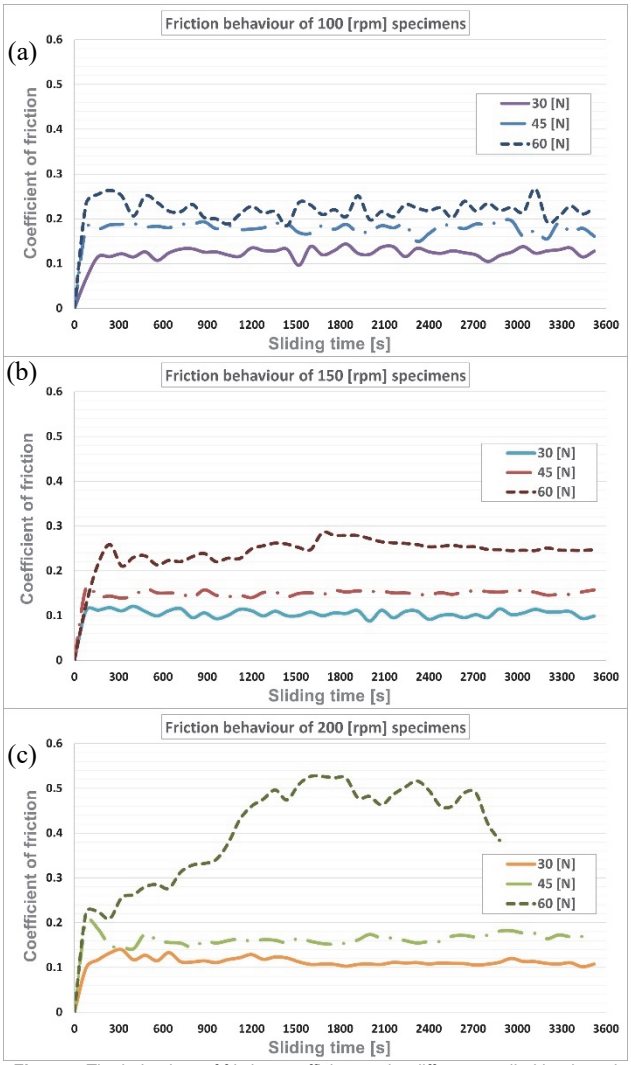

Figure 7 The behaviour of friction coefficient under different applied loads and testing speeds of (a) 100 rpm, (b) 150 rpm, and (c) 200 rpm

Fig. 7a to Fig. 7c displays the curves of friction coefficient of samples examined at three different speeds (100, 150, and 200 rpm), where each speed is under three loads (30, 45, 60 N). In general, the results within each speed alone show that the coefficient of friction was boosted as the load increases. Furthermore, a significant development in the friction coefficient was noticed (see Fig. 8c) when the highest speed (200 rpm) and the largest load (60 N) were applied. In this sample, the test was not completed up to the planned time (one hour) as the sample broke, likewise in its repetition. This indicates that these are the test parameters upper limits the maximal that the current test pieces could bear. Moreover, when comparing the effect of test speed, within each load alone, it seems that the friction coefficient fluctuated within the same level. Moreover, over all speeds, the friction coefficient was around (1.2) for 30 N samples, (1.7) for 45 N samples, and slightly above (2) for 60 N samples (except for 200 rpm where the friction was boosted unexpectedly and the sample broke). This intimates that the test load has much more influence on the friction coefficient (for MED610 material, PJM printed) than the test speed.

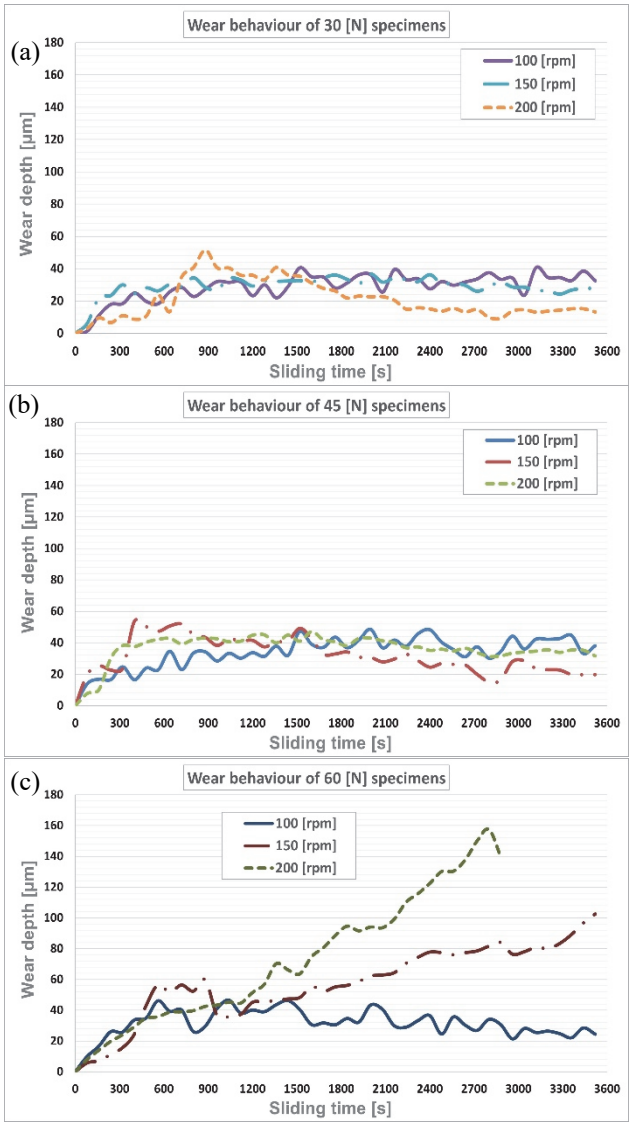

Figure 8 The development of wear depth under different testing speeds and applied load of (a) 30 N, (b) 45 N, and (c) 60 N

In terms of wear depth investigation, Fig. 8a to Fig. 8c presents the displacement results in µ] for samples examined under different test loads and speeds. Most of the samples reported a wear depth around 40 µm. However, an exception was observed in samples of the higher load (60 N) at 150 and 200 rpm speeds, as the wear depth of the 150 rpm speed's sample increased steadily along with the sliding time. Simultaneously, the wear in the 200 rpm speed's sample developed dramatically till the sample was fractured at 2900 s of the tribology test time.

A comparison of the average friction coefficient obtained in all tested conditions is exhibited in Fig. 9a. Here, the average value of friction coefficient could be estimated from the stable stage of the friction behaviour curve. Since some of the curves have no stable stage, hence, the function MODE.SNGL in Microsoft excel software was applied to determine the average value. This function returns the most regularly occurring number within a numeric data set. Thus, the average (most frequent number) of friction coefficient can be extracted. It can be clearly seen from Fig. 9a that, within each test speed alone, the average friction coefficient increased as the load lifted. Also, enhancing the test speed, in general, raised the friction coefficient as well.

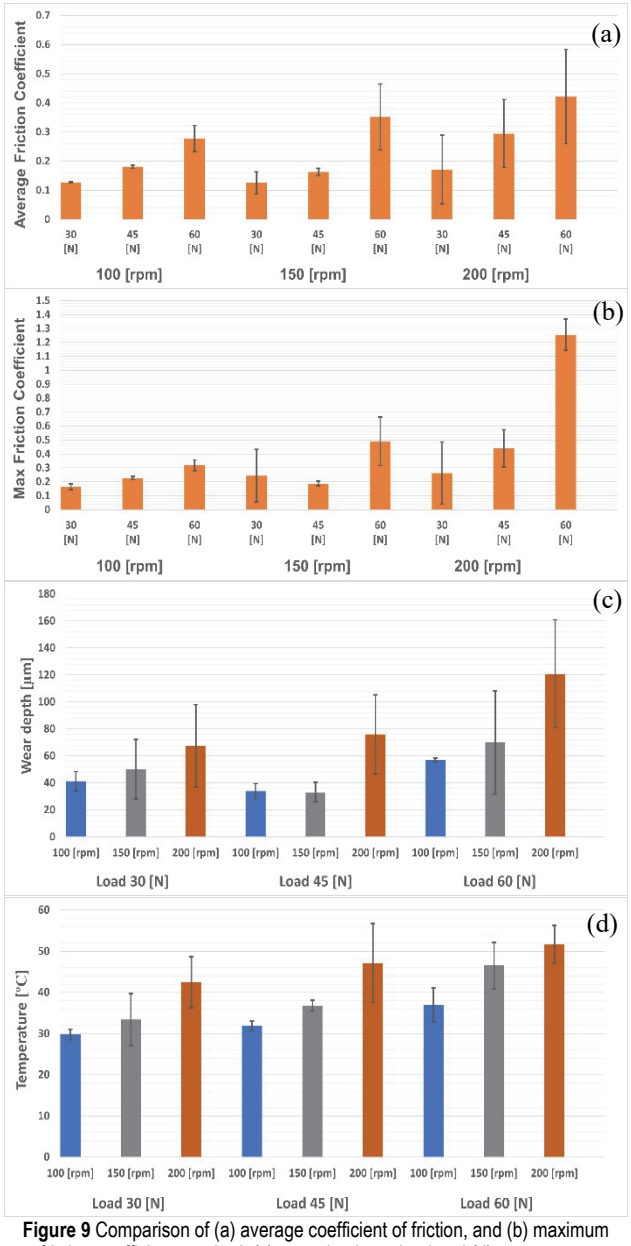

Figure 9 Comparison of (a) average coefficient of friction, and (b) maximum friction coefficient reached, (c) wear depth attained and (d) temperature development, for tribological samples tested under different speeds and applied loads

The maximum values of friction coefficient that were reached in samples tested under all experimented conditions are exposed in Fig. 9b. Accordingly, the maximum friction coefficient revealed a similar tendency as compared to the average friction coefficient, as it increased with the increase of load and speed. An exception was noticed in the trend of the sample under the 45 N load at a test speed of 150 rpm, where the maximum friction coefficient decreased rather than expanded.The average values of the coefficient of friction shown in Fig. 9 show that the highest values of this parameter are obtained for the speed of 200. This may be due to the increasing level of vibrations caused by the increased rotational speed. Moreover, for this value and the highest load, the samples were damaged, which means that these parameters are extreme values.

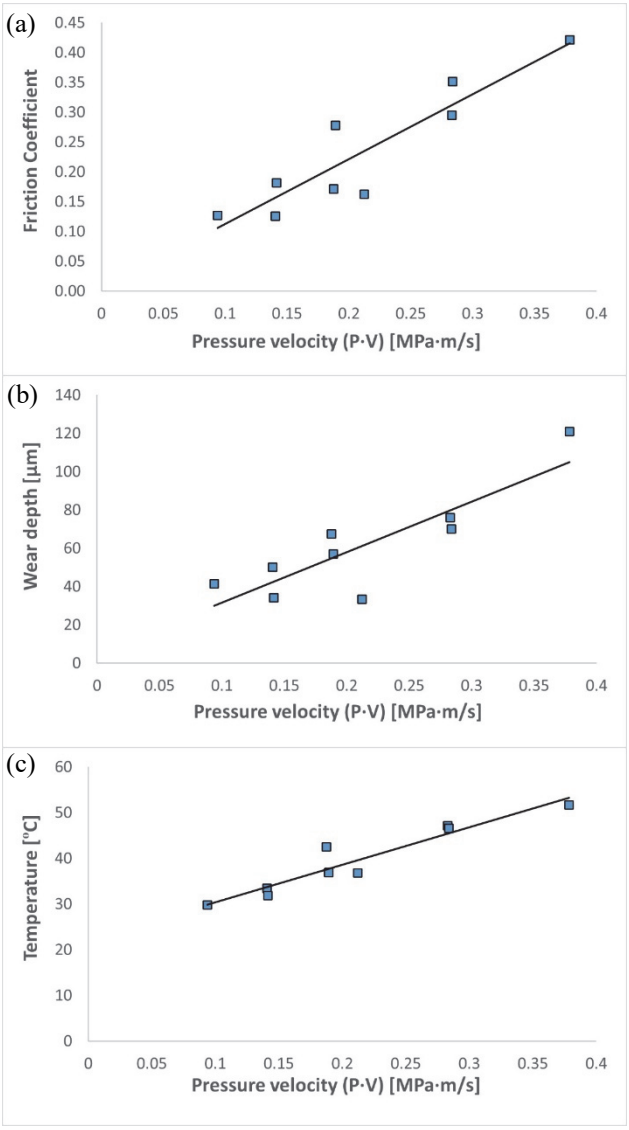

Figure 10 Pressure-velocity (*P.V*) vs. (a) friction coefficient, (b) wear depth and (c) temperature

Comparisons of wear depth attained among tribological samples experimented under different loads and speeds are shown in Fig. 9c. Although the wear depth value was supposed to be the last point of the curves, this was found to be non applicable due to the curve's continuous fluctuation. Therefore, for a more fair determination, the last 600 measurements (from 3000 to 3600 s) were averaged, and the wear depth value was then specified. For samples investigated under 30 and 60 N loads, the wear depth was found to enlarge with the increase of the test speed. However, under a load of 45 N, the 100 and 150 rpm speed samples offered an equally low wear depth.

The temperature development of tribological test pieces examined under different loads and speeds is presented in Fig. 9d. A consistent increment was detected, along with the increase of speed and load. This can be ascribed to the augmentation in the friction when load and speed increase, between the samples' surface and the tribology test's counterpart.

The *PV* factor (*P* (contact pressure) and *V* (sliding velocity)) is an important parameter in the tribology of materials. The influence of *PV* on the coefficient of friction, wear depth and rising heat (temperature) is presented in Fig. 10a to Fig. 10c, respectively. The friction coefficient increases with the growth of *PV* for the conditions investigated. This can be ascribed to the increase in the real area of contact due to the increasing contact pressure [28]. Moreover, the frictional or tangential forces between the asperities could be associated with the sliding velocity, thus, the friction coefficient increases with the increase in *PV* [33]. A comparable trend was observed regarding the effect of *PV* on the wear depth and temperature.

3.3 Metrology Investigation

Tribological test evaluation can also be performed based on the trace reflected on the surface texture. The friction pair, in a characteristic way, forms irregularities on the surface. The maximum depth and the area of the friction surface depend, among others, on the materials of the elements and the process parameters. Fig. 11 shows the selected wear profile in a cross-section sample 2b. The area of the friction surface shaped by dislodging of loose wear products can be noted in red on the figure. Moreover, plastic deformation was evidenced on selected samples under the influence of temperature.

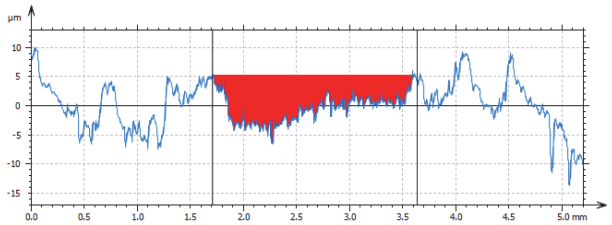

Figure 11 The wear profile in a cross-section sample 2b

Table 3 Metrological values for 27 samples.

Sample determination	Maximum depth / µm	Hole area / mm^2	
1a	23.47	0.0436028	
1b	30.41	0.035	
1c	31.87	0.094	
2a	15.52	0.009	
2b	12.11	0.011	
2c	8.43	0.001	
3a	9.22	0.004	
3b	destroyed sample		
3c	16.50	0.013	
4a	45.54	0.058	
4b	20.96	0.028	
4c	39.26	0.074	
5a	27.30	0.052	
5b	19.73	0.024	
5c	13.86	0.022	
6a	16.35	0.017	
6b	destroyed sample		
6c	31.83	0.011	
7a	37.41	0.034	
7b	47.61	0.078	
7c	23.72	0.026	
8a	destroyed sample		
8b	13.92	0.0098606	
8c	destroyed sample		
9a	destroyed sample		
9b			
9c			

The obtained values of the profile measurements by Talysurf CCI are summarized in Tab. 3. The greatest maximum depth was found for sample 7b. The value was

47.61 µm. The biggest hole area was found on sample 1c. The value was 94077 µm^2. Furthermore, it can be observed that both the maximum depth and the area of the friction surface decrease with increasing rotational speed. On the other hand, as the pressure parameter increases, the maximum depth increases, while the area of the friction surface decreases. This shows the nature of the surface texture changes and the different degree of wear of the samples depending on the process parameters.

Thus, as a result of too much wear, the average value of which was for sample 3b are142,91 µm, for sample 8a are 79,56 µm and for sample 8c are 46,32 µm, the samples were destroyed. In the case of sample 6b, the measuring instrument measured the sample several times over a distance of 2,20 mm. Samples 9a, 9b and 9c cracked during the tribological test and deformed plastically in the place where the metrological test should be performed, as shown in Fig. 12.

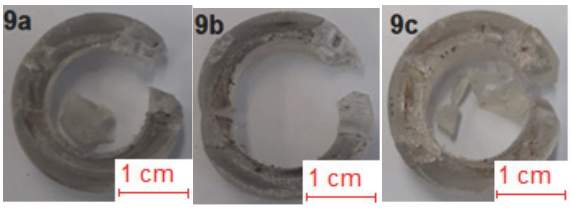

Figure 12 Broken samples 9a, 9b and 9c.

4 CONCLUSIONS

The paper describes the topic of tribological wear of sample models made with one of the most accurate 3D printing technologies based on photo-polymerization of liquid polymer resins. Both the pure data obtained from the friction test and the indirect metrological evaluation of the surfaces at the friction site after the end of the test were analyzed. By assessing the results of the research presented in this article, the following general conclusions can be formulated:

Based on the clean results of friction of samples made of MED610 in the PJM technology, it can be concluded that they are characterized by a relatively low resistance to abrasive wear. This opinion is confirmed by the *PV* diagram and damaged samples, which excludes its use in the production of models intended for heavily loaded friction nodes.

During the tests, the critical friction parameters were determined that resulted in the destruction of the sample models. When analyzing the *PV* graph, it can be stated that the value of the *PV* product increases linearly with the increase in both the pressure force and the speed, which is a typical phenomenon and the upward trend is maintained. For the samples with the highest *PV* association, the models were destroyed during the friction process, which was documented in the photographs presented. It seems that the critical value was exceeded and the test itself allowed to determine the maximum values that can be loaded on the sample while working in engineering applications.

The metrological analysis of the samples showed the importance of the selection of process parameters. The variability of the input data directly affected the shape and nature of the variability of the irregularities in a particular cross-section. We found that the maximum depth and the area of the friction surface decrease with increasing rotational speed. However, when the pressure parameter increases, the maximum depth increases, while the area of the friction surface decreases. In the future, the authors plan to conduct research for an increased range of rotational speeds and force, taking into account variable technological parameters such as the printing direction and the layer thickness, which will certainly allow for a better understanding of the tribological properties of the presented material.

Acknowledgements

The research was partially financed by the doctoral school at the Kielce University of Technology and the funds of the Faculty of Mechatronics and Machine Engineering at Kielce University of Technology. Moreover, this research was also partially funded by the National Science Center of Poland under the Miniatura 4, grant number 2020/04/X/ST5/00057 entitled: Analysis of polymer composites produced by 3D printing and electrospinning technologies in the applications of filtering devices.

5 REFERENCES

[1] Adamczak, S., Zmarzly, P., Kozior, T., & Gogolewski, D. (2017). Assessment of roundness and waviness deviations of elements produced by selective laser sintering technology. *Engineering mechanics 2017*.

[2] Alifui-Segbaya, F., Varma, S., Lieschke, G. J., & George, R. (2017). Biocompatibility of Photopolymers in 3D Printing. *3D Printing and Additive Manufacturing*, *4*(4), 185-191. https://doi.org/10.1089/3dp.2017.0064

[3] Aslani, K.-E., Vakouftsi, F., Kechagias, J. D., & Mastorakis, N. E. (2019). Surface Roughness Optimization of Poly-Jet 3D Printing Using Grey Taguchi Method. *2019 International Conference on Control, Artificial Intelligence, Robotics & Optimization (ICCAIRO)*, 213-218. https://doi.org/10.1109/ICCAIRO47923.2019.00041

[4] Bochnia, J., Blasiak, M., & Kozior, T. (2020). Tensile strength analysis of thin-walled polymer glass fiber reinforced samples manufactured by 3d printing technology. *Polymers*, *12*, 2783. https://doi.org/10.3390/polym12122783

[5] Bochnia, J., Blasiak, M., & Kozior, T. (2021). A Comparative Study of the Mechanical Properties of FDM 3D Prints Made of PLA and Carbon Fiber-Reinforced PLA for Thin-Walled Applications. *Materials*, *14*, 7062.

[6] Bochnia, J., & Blasiak, S. (2016). Anisotrophy of mechanical properties of a material which is shaped incrementally using polyjet technology. *Engineering mechanics 2016*.

[7] Budzik, G., Przeszlowski, L., Wieczorowski, M., Rzucidlo, A., Gapinski, B., & Krolczyk, G. (2018). Analysis of 3D printing parameters of gears for hybrid manufacturing. *AIP Conference Proceedings*, *1960*(140005). https://doi.org/10.1063/1.5034997

[8] Chan, Y.-W., Fang, H.-Y., Shie, M.-Y., & Shen, Y. F. (2019). The mussel-inspired assisted apatite mineralized on PolyJet material for artificial bone scaffold. *International Journal of Bioprinting*, *5*(2). https://doi.org/10.18063/ijb.v5i2.197

[9] Dziegielewski, W., Kowalczyk, J., Kulczycki, A., Madej, M., & Ozimina, D. (2020). Tribochemical interactions between carbon nanotubes and ZDDP antiwear additive during tribofilm formation on uncoated and DLC-Coated steel. *Materials*, *12*, 2409. https://doi.org/10.3390/ma13102409

[10] *EN ISO 10993-10:2013 Biological evaluation of medical devices - Part 10: Tests for irritation and skin sensitization*. (2013).
[11] *EN ISO 10993-18:2009 Biological evaluation of medical devices - Part 18: Chemical characterization of materials*. (2009).
[12] *EN ISO 10993-3:2014 Biological evaluation of medical devices - Part 3: Tests for genotoxicity, carcinogenicity and reproductive toxicit*. (2014).
[13] *EN ISO 10993-5:2009 Biological evaluation of medical devices - Part 5: Tests for in vitro cytotoxicity*. (2009).
[14] Gogolewski, D., Bartkowiak, T., Kozior, T., & Zmarzły, P. (2021). Multiscale analysis of surface texture quality of models manufactured by laser powder-bed fusion technology and machining from 316l steel. *Materials*, *14*(11), 2794. https://doi.org/10.3390/ma14112794
[15] Gong, X., Dang, R., Xu, T., Yu, Q., & Zheng, J. (2020). Full Digital Workflow of Nasoalveolar Molding Treatment in Infants With Cleft Lip and Palate. *Journal of Craniofacial Surgery*, *31*(2), 367-371. https://doi.org/10.1097/SCS.0000000000006258
[16] Gouzman, I., Atar, N., Grossman, E., Verker, R., Bolker, A., Pokrass, M., Sultan, S., Sinwani, O., Wagner, A., Lück, T., & Seifarth, C. (2019). 3D Printing of Bismaleimides: From New Ink Formulation to Printed Thermosetting Polymer Objects. *Advanced Materials Technologies*, *4*(10), 1900368. https://doi.org/10.1002/admt.201900368
[17] Guo, N. & Leu, M. C. (2013). Additive manufacturing: Technology, applications and research needs. *Frontiers of Mechanical Engineering*, *8*(3), 215-243. https://doi.org/10.1007/s11465-013-0248-8
[18] Hanon, M. M., Marczis, R., & Zsidai, L. (2020). Impact of 3D-printing structure on the tribological properties of polymers. *Industrial Lubrication and Tribology*, *72*(6), 811-818. https://doi.org/10.1108/ILT-05-2019-0189
[19] Hanon, M. M. & Zsidai, L. (2021). Comprehending the role of process parameters and filament color on the structure and tribological performance of 3D printed PLA. *Journal of Materials Research and Technology*, *15*, 647-660. https://doi.org/10.1016/j.jmrt.2021.08.061
[20] Kechagias, J., Stavropoulos, P., Koutsomichalis, A., Ntintakis, I., & Vaxevanidis, N. (2014). Dimensional Accuracy Optimization of Prototypes produced by PolyJet Direct 3D Printing Technology. *Advances in Engineering Mechanics and Materials: (International Conference on Industrial Engineering-Inde 2014)*, 61-65.
[21] Kozior, T. (2020). The Influence of Selected Selective Laser Sintering Technology Process Parameters on Stress Relaxation, Mass of Models, and Their Surface Texture Quality. *3D Printing and Additive Manufacturing*, *7*(3), 126-138. https://doi.org/10.1089/3dp.2019.0036
[22] Kozior, T., & Kundera, C. (2021). Rheological properties of cellular structures manufactured by additive PJM technology. *Tehnicki Vjesnik*, *28*(1), 82-87. https://doi.org/10.17559/TV-20191007145545
[23] Kozior, T., & Kundera, C. (2021). Viscoelastic Properties of Cell Structures Manufactured Using a Photo-Curable Additive Technology-PJM. *Polymers*, *13*(11), 1895. https://doi.org/10.3390/polym13111895
[24] Kozior, T., Mamun, A., Trabelsi, M., Sabantina, L., & Ehrmann, A. (2020). Quality of the surface texture and mechanical properties of FDM printed samples after thermal and chemical treatment. *Strojniski Vestnik/Journal of Mechanical Engineering*, *66*(2), 105-113. https://doi.org/10.5545/sv-jme.2019.6322
[25] Maurya, N. K., Rastogi, V., & Singh, P. (2021). Experimental and computational analysis of mechanical properties of RGD840 material manufactured through PolyJet process. *Rapid Prototyping Journal*, *27*(1), 207-214. https://doi.org/10.1108/RPJ-03-2020-0049
[26] Mueller, J., Shea, K., & Daraio, C. (2015). Mechanical properties of parts fabricated with inkjet 3D printing through efficient experimental design. *Materials & Design*, *86*, 902-912. https://doi.org/10.1016/j.matdes.2015.07.129
[27] Ngan, C. G. Y., O'Connell, C. D., Blanchard, R., Boyd-Moss, M., Williams, R. J., Bourke, J., Quigley, A., McKelvie, P., Kapsa, R. M. I., & Choong, P. F. M. (2019). Optimising the biocompatibility of 3D printed photopolymer constructs in vitro and in vivo. *Biomedical Materials*, *14*(3), 035007. https://doi.org/10.1088/1748-605X/ab09c4
[28] Pei, X.-Q., Lin, L., Schlarb, A. K., & Bennewitz, R. (2019). Correlation of friction and wear across length scales for PEEK sliding against steel. *Tribology International*, *136*, 462-468. https://doi.org/10.1016/j.triboint.2019.04.001
[29] Pugalendhi, A., Ranganathan, R., & Chandrasekaran, M. (2020). Effect of process parameters on mechanical properties of VeroBlue material and their optimal selection in PolyJet technology. *The International Journal of Advanced Manufacturing Technology*, *108*(4), 1049-1059. https://doi.org/10.1007/s00170-019-04782-z
[30] Saharudin, M. S., Hajnys, J., Kozior, T., Gogolewski, D., & Zmarzły, P. (2021). Quality of Surface Texture and Mechanical Properties of PLA and PA-Based Material Reinforced with Carbon Fibers Manufactured by FDM and CFF 3D Printing Technologies. *Polymers*, *13*, 1671. https://doi.org/https://doi.org/10.3390/polym13111671
[31] Sanders, J., Wei, X., & Pei, Z. (2021). Experimental Investigation of PolyJet 3D Printing: Effects of Sample Location and Volume on Power Consumption. *Manufacturing Letters*. https://doi.org/10.1016/j.mfglet.2021.07.013
[32] Spahiu, T., Al-Arabiyat, M., Martens, Y., Ehrmann, A., Piperi, E., & Shehi, E. (2018). Adhesion of 3D printing polymers on textile fabrics for garment production. *IOP Conference Series: Materials Science and Engineering*. https://doi.org/10.1088/1757-899X/459/1/012065
[33] Srinath, G., & Gnanamoorthy, R. (2005). Effect of Short Fibre Reinforcement on the Friction and Wear Behaviour of Nylon 66. *Applied Composite Materials*, *12*(6), 369-383. https://doi.org/10.1007/s10443-005-5824-6
[34] Stratasys. (2018). Biocompatible Clear MED610 Data Sheet. In *Technical Datasheet* (Issue 4).
[35] Tee, Y. L., Peng, C., Pille, P., Leary, M., & Tran, P. (2020). PolyJet 3D Printing of Composite Materials: Experimental and Modelling Approach. *JOM*, *72*(3), 1105-1117. https://doi.org/10.1007/s11837-020-04014-w
[36] Vidakis, N., Petousis, M., Vaxevanidis, N., & Kechagias, J. (2020). Surface Roughness Investigation of Poly-Jet 3D Printing. *Mathematics*, *8*(10), 1758. https://doi.org/10.3390/math8101758
[37] Wagner, A., Gouzman, I., Atar, N., Grossman, E., Pokrass, M., Fuchsbauer, A., Schranzhofer, L., & Paulik, C. (2019). Cure kinetics of bismaleimides as basis for polyimide-like inks for PolyJet™-3D-printing. *Journal of Applied Polymer Science*, *136*(12), 47244. https://doi.org/10.1002/app.47244
[38] Zmarzły, P. (2020). Technological heredity of the turning process. *Tehnicki Vjesnik*, *27*(4), 1194-1203. https://doi.org/10.17559/TV-20190425150325

Contact information:

Mateusz RUDNIK, PhD candidate
Kielce University of Technology,
Al. 1000-lecia P. P. 7, 25-314 Kielce, Poland
E-mail: mrudnik@tu.kielce.pl

Muammel M. HANON, PhD candidate
SzentIstván Campus, MATE University,
PáterKároly u. 1, 2100 Gödöllő, Hungary
Middle Technical University (MTU), Baquba Technical Institute,
Muasker Al Rashid St., 10074 Baghdad, Iraq
E-mail: sharba.muammel.m.hanon@phd.uni-szie.hu

Wiktor SZOT, PhD candidate
Kielce University of Technology,
Al. 1000-lecia P. P. 7, 25-314 Kielce, Poland
E-mail: wszot@tu.kielce.pl

Karolina BECK, MSc student and PhD candidate
Kielce University of Technology,
Al. 1000-lecia P. P. 7, 25-314 Kielce, Poland
E-mail: kbeck@tu.kielce.pl

Damian GOGOLEWSKI, PhD
Kielce University of Technology,
Al. 1000-lecia P. P. 7, 25-314 Kielce, Poland
E-mail: dgogolewski@tu.kielce.pl

Pawe ŁZMARZŁY, PhD
Kielce University of Technology,
Al. 1000-lecia P. P. 7, 25-314 Kielce, Poland
E-mail: pzmarzly@tu.kielce.pl

Tomasz KOZIOR, PhD
(Corresponding author)
Kielce University of Technology,
Al. 1000-lecia P. P. 7, 25-314 Kielce, Poland
E-mail: tkozior@tu.kielce.pl